Bond Angle Effects on the Migratory Insertion of Ethylene and Carbon Monoxide into Palladium(II)−Methyl Bonds in Complexes Bearing Bidentate Phosphine Ligands

John Ledford, C. Scott Shultz, Derek P. Gates, Peter S. White, Joseph M. DeSimone, and Maurice Brookhart*

Department of Chemistry, University of North Carolina at Chapel Hill, Chapel Hill, North Carolina 27599-3290

Received June 8, 2001

Labile (P−P)Pd(CH_3)(OEt_2)$^+$$BAr'_4{}^-$ complexes (**2**) have been prepared via protonation of (P−P)$PdMe_2$ (**1**), where P−P = *cis*-1,2-bis(diphenylphosphino)ethylene (**a**, dppee), 1,2-bis(diphenylphosphino)benzene (**b**, dpbz), 1,2-bis(diphenylphosphino)ethane (**c**, dppe), 1,2-bis(dimethylphosphino)ethane (**d**, dmpe), 1,3-bis(diphenylphosphino)propane (**e**, dppp), 1,3-bis(diisopropylphosphino)propane (**f**, dippp), 1,4-bis(diphenylphosphino)butane (**g**, dppb) and Ar′ = 3,5-$(CF_3)_2C_6H_3$. Unstable complex **2d** (P−P = dmpe) was generated in situ. X-ray structures are reported for **1e** and **2e**−**g**. Treatment of **2a**−**g** with CO in CH_2Cl_2 at −90 °C yields the (P−P)Pd(CH_3)(CO)$^+$ complexes **3a**−**g**. Barriers to migratory insertion in **3a**−**g** were determined with the ordering to be: **3f** (dippp) ≈ **3g** (dppb) < **3e** (dppp) ≪ **3a** (dppee) ≈ **3b** (dpbz) ≈ **3c** (dppe) < **3d** (dmpe). Exposure of **2a**−**g** to ethylene at −80 °C yields the ethylene complexes (P−P)Pd(CH_3)(C_2H_4)$^+$ (**5a**−**g**). Barriers to migratory insertion in these complexes were determined by NMR spectroscopy to be: **5b** (dpbz) ≈ **5e** (dppp) ≈ **5f** (dippp) ≈ **5g** (dppb) < **5a** (dppee) ≈ **5c** (dppe) < **5d** (dmpe). Complexes (P−P)Pd(CH_2CH_3)(C_2H_4)$^+$ (**6a**−**e**,**g**) produced from **5a**−**e**,**g** under C_2H_4 are catalyst resting states for the dimerization of C_2H_4 to butenes. In the case of **5f** (P−P = dippp), the catalyst resting state produced is the β-agostic ethyl complex (dippp)Pd(CH_2CH_2-μ-H)$^+$ (**8f**), which has been isolated. This complex exhibits two dynamic processes studied by VT-NMR: interchange of C_α and C_β ($\Delta G^\ddagger$ = 10.3(2) kcal/mol) and rotation of the agostic methyl group ($\Delta G^\ddagger$ ca. 6.4 kcal/mol). The β-agostic propyl complex **7f** has been generated and identified as the *n*-propyl isomer (dippp)Pd(CH_2CH_2-μ-HCH_3)$^+$.

Introduction

Cationic palladium(II) complexes bearing neutral bidentate ligands are excellent catalysts for the alternating copolymerization of CO and olefins as well as olefin dimerization, particularly dimerization of ethylene to butenes.[1−5] The fundamental steps in these transformations involve the migratory insertion reactions of alkyl carbonyl, acyl olefin, and alkyl olefin species as shown in eqs 1−3.

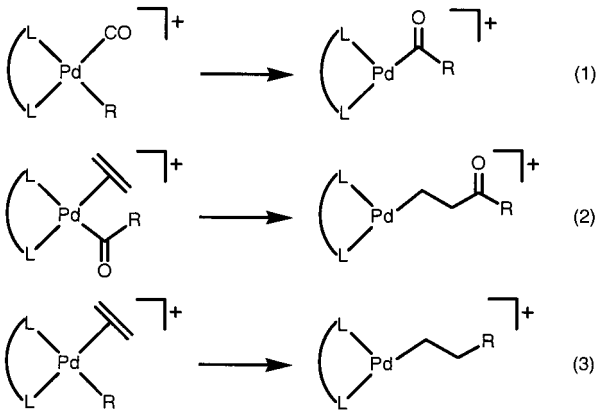

Such migratory insertion reactions are members of a larger class of transition-metal-mediated C−C bond forming reactions that are observed in processes such as hydroformylation, hydroesterification, olefin oligomerization, and polymerization. Several groups, including ours, have examined aspects of these insertion reactions employing Pd(II) systems containing bidentate nitrogen ligands.[6−9] For example, we have measured the free energies of activation for migratory insertion for the series (phen)Pd(CH_3)(CO)$^+$$BAr'_4{}^-$, (phen)Pd($CH_3$)($C_2H_4$)$^+$$BAr'_4{}^-$, (phen)Pd($CH_2CH_3$)($C_2H_4$)$^+$$BAr'_4{}^-$, and (phen)Pd($COCH_3$)($C_2H_4$)$^+$$BAr'_4{}^-$ (phen = η^2-1,10-phenanthroline, $BAr'_4{}^-$ = B(3,5-$C_6H_3(CF_3)_2)_4{}^-$) and, in combination with other kinetic and thermodynamic studies, have constructed a complete catalytic cycle for the copolymerization of ethylene and CO using the phenanthroline-based Pd(II) system.[7,8]

Since commercial catalyst systems for the production of ethylene/CO copolymers have used bidentate phosphine ligands,[10,11] we have recently focused our atten-

(1) Drent, E. *Pure Appl. Chem.* **1990**, *62*, 661.
(2) Drent, E.; van Broekhoven, J. A. M.; Doyle, J. J. *J. Organomet. Chem.* **1991**, *417*, 235.
(3) Sen, A. *Acc. Chem. Res.* **1993**, *26*, 303.
(4) Sen, A.; Jiang, Z. *Macromolecules* **1993**, *26*, 911.
(5) For reviews see: Drent, E.; Budzelaar, P. H. M. *Chem. Rev.* **1996**, *96*, 663. Sommazzi, A.; Garbassi, F. *Prog. Polym. Sci.* **1997**, *22*, 1547. Sen, A. *Adv. Polym. Sci.* **1986**, *73*−*74*, 125.

10.1021/om010489k CCC: $20.00
Publication on Web 11/07/2001

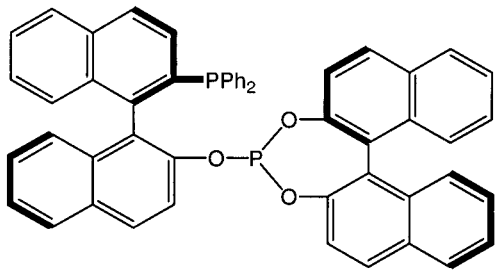

(*R*, *S*)-BINAPHOS

Figure 1. Chiral phosphine−phosphite used by Nozaki et al.

tion on studying the fundamental migratory insertion reactions (eqs 1−3) of palladium complexes containing bidentate phosphine based ligands, specifically the 1,3-bis(diphenylphosphino)propane (dppp) ligand.[12] We have now extended this study to examine a series of bidentate phosphine ligands to determine the effects that changing the structural and/or electronic properties of the ligand have on migratory insertion processes. An intriguing observation concerning the overall catalytic activity of these systems in the copolymerization of ethylene and carbon monoxide is that the size of the chelate ring dramatically affects productivity, with the most productive catalyst being the one with a ligand containing a three-carbon backbone.[5,13]

A number of studies concerning the insertion of CO into $Pd^{II}-CH_3$ bonds in $(P-P)Pd^{II}$ complexes have been reported. Dekker et al. have examined the reactions of the series of complexes $[(C_6H_5)_2P(CH_2)_nP(C_6H_5)_2]Pd(CH_3)(Cl)$ and $[(C_6H_5)_2P(CH_2)_nP(C_6H_5)_2]Pd(CH_3)(CH_3CN)^+$ with CO to yield acyl complexes.[13] Qualitative rate differences were observed with $(n = 4) \geq (n = 3) \gg (n = 2)$. In these studies, conversion of the starting complexes to acyl derivatives involves first the displacement of Cl^- (or CH_3CN) by CO to yield the unobserved $(P-P)Pd(CH_3)(CO)^+$ followed by methyl migration to form the acyl product. Since the $(P-P)Pd(CH_3)(CO)^+$ complexes are not directly observed, it is not clear how the half-lives of the overall transformations relate to the primary migratory insertion step (eq 1). A similar experiment reported by Nozaki et al.[14] revealed the $\Delta G^{\ddagger}$ value for the conversion of the chelate complex ((*R*,*S*)-BINAPHOS)$\overline{\text{PdCH}_2\text{CH(CH}_3\text{)C(O)CH}_3}^+$ to the acyl−acetonitrile complex ((*R*,*S*)-BINAPHOS)$Pd(NCCH_3)(C(O)CH_2CH(CH_3)C(O)CH_3)^+$ to be ca. 19 kcal/mol (Figure 1). There is most likely a significant energy cost for initial chelate opening in this case to form the intermediate $(P-P)Pd(R)(CO)^+$ prior to insertion. Thus, again, the primary insertion barrier is not known. We have previously measured the barrier of migratory insertion in complex **3a**, $(dppp)Pd(CH_3)(CO)^+$, to yield $\Delta G^{\ddagger} = 14.8$ kcal/mol,[12] which is consistent with that observed qualitatively by Tòth and Elsevier, who reported the in situ generation of [(2*S*,4*S*)-2,4-bis(diphenylphosphino)pentane]$Pd(CH_3)(CO)^+$ and observed the half-life for migratory insertion, which was indicative of a $\Delta G^{\ddagger}$ value of ∼14−15 kcal/mol.[15]

There have been several theoretical treatments of the migratory insertion processes noted in eqs 1−3. Thorn and Hoffman's extended Hückel analysis illustrated that for the migratory insertion of $(PH_3)_2Pt(H)(C_2H_4)^+$ the P−Pt−P angle goes from 95° in the starting cis complex through 110° in the transition state.[16] This suggests that an appropriate bidentate phosphine ligand with a P−Pt−P bond angle close to 110° would help to destabilize the ground state with respect to the transition state, thereby reducing the activation barrier. Widening of the $F-Pt-PH_3$ angle was also predicted by Sakaki et al. to occur in the transition state for migratory insertion of $(PH_3)(F)Pt(CH_3)(CO)$ on the basis of ab initio Hartree−Fock calculations.[17] Ziegler et al. used *cis*-$H_2PCH{=}CHPH_2$ as the model bidentate ligand and calculated barriers for migratory insertion in $(P-P)Pd(C_2H_5)(CO)^+$ and $(P-P)Pd(C_2H_5)(C_2H_4)^+$ of 11.5 and 15.6 kcal/mol, respectively.[18,19] Morokuma and co-workers carried out calculations using the diimine ligand HN=CHCH=NH as the model bidentate ligand and predicted barriers of insertion for $(HN{=}CHCH{=}NH)Pd(CH_3)(CO)^+$ and $(HN{=}CHCH{=}NH)Pd(CH_3)(C_2H_4)^+$ of 14.9 and 16.2 kcal/mol, respectively.[20,21]

In this paper we report detailed investigations of the generation of complexes of the general formula $(P-P)Pd(CH_3)(CO)^+$ and $(P-P)Pd(R)(C_2H_4)^+$ (R = $-CH_3$, $-CH_2CH_3$) and the measurement of the barriers to migratory insertion employing a variety of bidentate phosphine ligands, **a**−**g** (shown in Figure 2). These results provide quantitative information regarding these barriers, with specific attention being paid to the role of the P−Pd−P bond angle and donor properties of the bidentate phosphine ligand. The catalytic cycle for ethylene dimerization has been investigated; the catalyst resting state is shown to be a function of the structure of the bidentate phosphorus ligand.

Results and Discussion

1. Synthesis of Diethyl Ether Adducts, $(P-P)Pd(CH_3)(OEt_2)^+$ BAr'_4^- (Ar′ = 3,5-$(CF_3)_2C_6H_3$; 2a−g). A series of seven bidentate phosphine ligands, including the previously studied 1,3-bis(diphenylphosphino)propane (dppp) ligand,[12] was selected for the present study (see Figure 2). Analogous to previous work employing bidentate nitrogen ligands,[7−9,22,23] ether adducts of the

(6) Rülke, R. E.; Delis, J. G. P.; Groot, A. M.; Elsevier, C. J.; van Leeuwen, P. W. N. M.; Vrieze, K.; Goubitz, K.; Schenk, H. *J. Organomet. Chem.* **1996**, *508*, 109.
(7) Rix, F. C.; Brookhart, M. *J. Am. Chem. Soc.* **1995**, *117*, 1137.
(8) Rix, F. C.; Brookhart, M.; White, P. S. *J. Am. Chem. Soc.* **1996**, *118*, 4746.
(9) Brookhart, M.; Rix, F. C.; DeSimone, J. M. *J. Am. Chem. Soc.* **1992**, *114*, 5894.
(10) Mul, W. P.; Oosterbeek, H.; Beitel, G. A.; Kramer, G.-J.; Drent, E. *Angew. Chem., Int. Ed.* **2000**, *39*, 1848.
(11) Drent, E.; Budzelaar, P. H. M. *Chem. Rev.* **1996**, *96*, 663.
(12) Shultz, C. S.; Ledford, J.; DeSimone, J. M.; Brookhart, M. *J. Am. Chem. Soc.* **2000**, *122*, 6351.
(13) Dekker, G. P. C. M.; Elsevier, C. J.; Vrieze, K.; van Leeuwen, P. W. N. M. *Organometallics* **1992**, *11*, 1598.
(14) Nozaki, K.; Sato, N.; Tonomura, Y.; Yasutomi, M.; Takaya, H.; Hiyama, T.; Matsubara, T.; Koga, N. *J. Am. Chem. Soc.* **1997**, *119*, 12779.
(15) Tóth, I.; Elsevier, C. J. *J. Am. Chem. Soc.* **1993**, *115*, 10388.
(16) Thorn, D. L.; Hoffmann, R. *J. Am. Chem. Soc.* **1978**, *100*, 2079.
(17) Sakaki, S.; Kitaura, K.; Morokuma, K.; Ohkubo, K. *J. Am. Chem. Soc.* **1983**, *105*, 2280.
(18) Margl, P.; Ziegler, T. *Organometallics* **1996**, *15*, 5519.
(19) Margl, P.; Ziegler, T. *J. Am. Chem. Soc.* **1996**, *118*, 7337.
(20) Koga, M.; Morokuma, K. *J. Am. Chem. Soc.* **1986**, *108*, 6136.
(21) Svensson, M.; Matsubara, T.; Morokuma, K. *Organometallics* **1996**, *15*, 5568.
(22) Johnson, L. K.; Killian, C. M.; Brookhart, M. *J. Am. Chem. Soc.* **1995**, *117*, 6414.
(23) Tempel, D. J.; Brookhart, M. *Organometallics* **1998**, *17*, 2290.

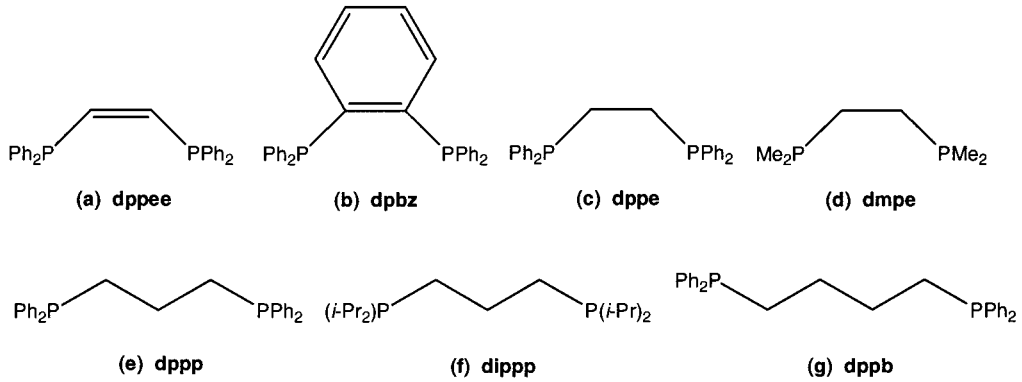

Figure 2. Bidentate phosphine ligands studied.

Table 1. Selected NMR Data[a] for (P−P)PdCH$_3$(OEt$_2$)$^+$BAr′$_4^-$

	2a	2b	2c	2d	2e	2f	2g
P−P	dppee	dpbz	dppe	dmpe	dppp	dippp	dppb
			^{1}H NMR				
[Pd]−C*H*$_3$[b]	0.63 (d, 7)	0.62 (d, 7)	0.52 (d, 7)	−	0.44 (d, 4)	0.59 (br)	0.69 (d, 7)
			^{13}C NMR				
[Pd]−*C*H$_3$[c]	12.3 (d, 88)	13.8 (d, 68)	12.2 (d, 86)	−	15.0 (d, 86)	7.7 (d, 79)	16.5 (d, 87)
			^{31}P NMR				
(*P*−*P*)[Pd][d]	61.2 (br)	57.1 (br)	60.1 (d, 25)	−	30.3 (d, 51)	55.3 (d, 38)	36.6 (br)
	49.2 (br)	41.2 (d, 26)	36.8 (d, 25)	−	−0.2 (d, 51)	11.0 (d, 38)	18.8 (br)

[a] Spectra were collected in CD_2Cl_2 at −80 °C. Chemical shift values (δ) are relative to CD_2Cl_2. All couplings (given in parentheses) are in Hz. [b] Couplings are $^3J_{HP}$. [c] Couplings are $^2J_{CP}$. [d] Couplings are $^2J_{PP}$.

palladium methyl cations, (P−P)Pd(CH$_3$)(OEt$_2$)$^+$, proved to be excellent precursors for generating a number of reactive catalytic intermediates through displacement of the labile ether ligand at low temperatures. The dimethyl complexes **1a**−**g**, some of which are known,[24−28] were prepared by a modification of the method previously reported by van Koten et al.[24] through displacement of TMEDA from (TMEDA)Pd(Me)$_2$ in acetone at 25 °C. Compounds **2a**−**g** were prepared by protonation of the dimethyl complexes with H(Et$_2$O)$_2$BAr′$_4$ in a mixture of diethyl ether and CH_2Cl_2 at −30 °C (eq 4).[12]

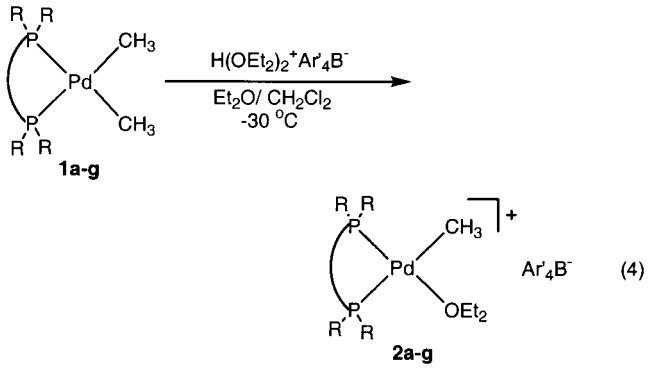

(4)

With the exception of the dmpe complex **2d**, the ether adducts were readily isolated and characterized by ^{1}H, ^{13}C, and ^{31}P NMR spectroscopy (Table 1) and can be stored for months as solids at −30 °C and withstand temperatures up to 25 °C for hours. Complex **2d** was unstable even at low temperatures (ca. −80 °C) and could not be characterized by ^{1}H or ^{31}P NMR spectroscopy; however, CO and olefin derivatives of **2d** could be prepared in a satisfactory manner from in situ prepared **2d**. In methylene chloride solution, complex **2g** containing the dppb ligand decays to other Pd(II) methyl complexes in the temperature range of −40 to 5 °C, depending on concentration. Traces of excess ligand appear to accelerate this process. Similar behavior was observed by van Leeuwen[13,29] and was attributed to dechelation of the poorly chelating dppb ligand and formation of complexes involving dppb as a bridging ligand. The ether adduct **2g** could be handled without problems from decay in a CH_2Cl_2/Et$_2$O mixture at or below 5 °C and in dilute solutions of CD_2Cl_2 below −40 °C.

Table 2. Selected Bond Distances (Å) and Angles (deg) of Complexes 1e and 2e−g

	1e	2e	2f	2g
		Distances		
Pd−CH$_3$	2.099(9)	2.065(5)	2.082(6)	2.062(9)
Pd−CH$_3$	2.092(11)			
Pd−O		2.204(3)	2.226(4)	2.226(5)
Pd−P1	2.307(3)	2.3615(16)	2.3865(23)	2.392(3)
Pd−P2	2.311(3)	2.1985(16)	2.2069(18)	2.2039(24)
		Angles		
CH$_3$−Pd−CH$_3$	85.9(4)			
CH$_3$−Pd−O1		88.74(16)	86.13(22)	85.7(3)
P1−Pd−P2	93.91(9)	97.26(6)	97.66(7)	102.42
P1−Pd−CH$_3$	90.1(3)			
P2−Pd−CH$_3$	90.0(3)	83.73(15)	83.53(20)	81.20(24)
P1−Pd−O1		90.59(9)	92.65(11)	90.93(17)

2. Structural Characterization of Complexes 1e and 2e−g by X-ray Crystallography. The lack of

(24) de Graff, W.; Boersma, J.; Smeets, W. J. J.; Spek, A. L.; van Koten, G. *Organometallics* **1989**, *8*, 2907.
(25) Ito, T.; Tsuchiya, H.; Yamamoto, A. *Bull. Chem. Soc. Jpn.* **1977**, *50*, 1319.
(26) Ozawa, F.; Yamamoto, A. *Nippon Kagaku Kaishi* **1987**, *5*, 773.
(27) Tooze, R.; Chiu, K. W.; Wilkinson, G. *Polyhedron* **1984**, *3*, 1025.
(28) Fryzuk, M. D.; Clentsmith, G. K. B.; Rettig, S. J. *J. Chem. Soc., Dalton Trans.* **1998**, 2007.
(29) Dekker, G. P. C. M.; Elsevier, C. J.; Vrieze, K.; van Leeuwen, P. W. N. M.; Roobeek, C. F. *J. Organomet. Chem.* **1992**, *430*, 357.

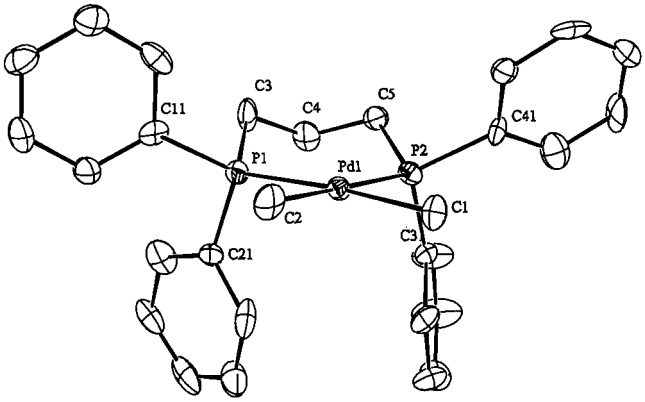

Figure 3. Crystal structure of (dppp)Pd(CH_3)$_2$ (**1e**). All atoms are drawn as 50% probability ellipsoids.

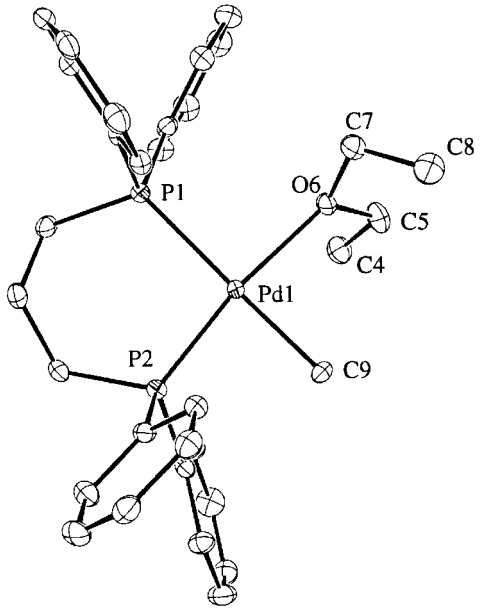

Figure 4. Crystal structure of (dppp)Pd(CH_3)(OEt_2)$^+$BAr′$_4^-$ (**2e**). The counterion is not shown for clarity. All atoms are drawn as 50% probability ellipsoids.

structural data for dialkyl complexes and methyl ether cations led us to characterize complexes **1e** and **2e**−**g** by X-ray diffraction. The molecular structures of the neutral dimethyl complex **1e** and the cationic methyl diethyl ether complexes **2e**−**g** are shown in Figures 3−6, respectively. Selected bond distances and angles are summarized in Table 2.

These structures provide useful information concerning the P−Pd−P bond angles in the monocationic systems and how they compare to the neutral systems. The structures of **2e**,**f** containing −(CH_2)$_3$− bridges are quite similar with P−Pd−P bond angles of ca. 97° (Figures 4 and 5) which are significantly larger than the ideal 90° for a square-planar complex. The ether complex **2g** with a −(CH_2)$_4$− bridge shows an even larger P−Pd−P bond angle of 102°, as expected (Figure 6). Other neutral Pd(II) complexes containing the dppp ligand show somewhat smaller P−Pd−P angles relative to **2e**: (dppp)$PdCl_2$ (90.6°)[30] and (dppp)Pd(NCS)$_2$ (89.3°).[31]

(30) Paviglianiti, A. J.; Minn, D. J.; Fultz, W. C.; Burmeister, J. L. *Inorg. Chim. Acta* **1989**, *159*, 65.
(31) Palenik, G. J.; Mathew, M.; Steffen, W. L.; Beran, G. *J. Am. Chem. Soc.* **1975**, *97*, 1059.

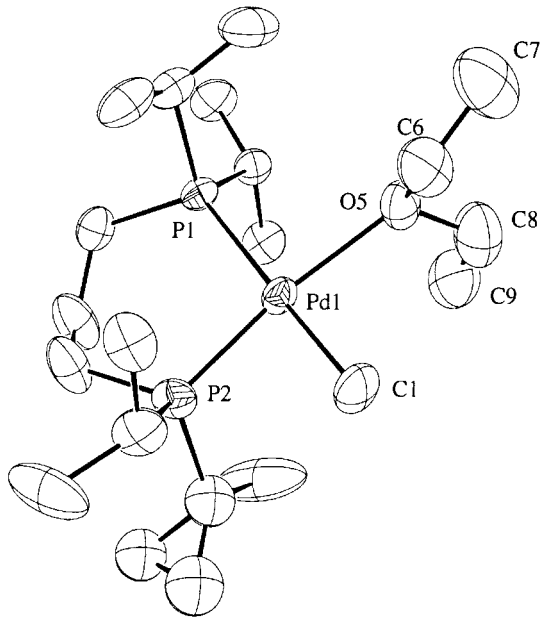

Figure 5. Crystal structure of (dippp)Pd(CH_3)(OEt_2)$^+$BAr′$_4^-$ (**2f**). The counterion is not shown for clarity. All atoms are drawn as 50% probability ellipsoids.

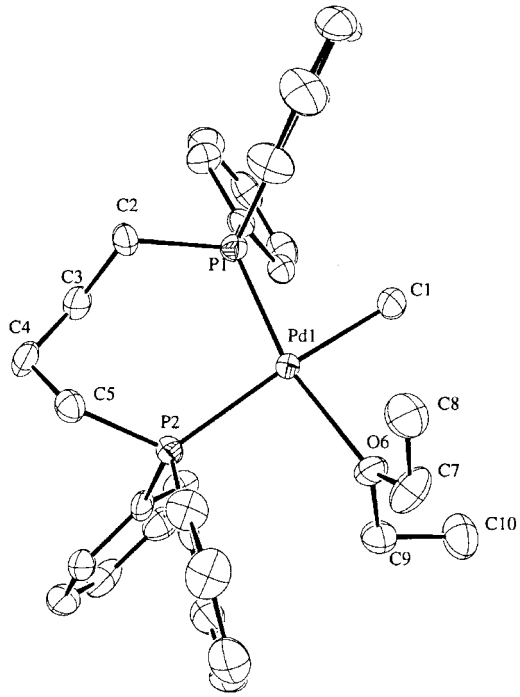

Figure 6. Crystal structure of (dppb)Pd(CH_3)(OEt_2)$^+$BAr′$_4^-$ (**1g**). The counterion is not shown for clarity. All atoms are drawn as 50% probability ellipsoids.

The differing trans effects of the diethyl ether and methyl ligands are reflected in the Pd−P bond distances. The Pd−P_2 bond distances (P_2 trans to Et_2O) in **2e**−**g** are ca. 0.16−0.19 Å shorter than the Pd−P_1 distance (P_1 trans to −CH_3), consistent with the fact that CH_3^- is a much stronger σ-donor ligand than Et_2O. As expected on steric grounds, the ether ligands lie perpendicular to the square plane. However, an unusual feature of ether complexes **2e**−**g** is that the ether ligand adopts a gauche conformation around one of the C−O bonds (for example, see the C_7−O_6 axis in Figure 4). This is in contrast to the ether ligand in (1,10-

Table 3. Selected NMR and IR Data[a] for (P−P)PdCH$_3$(CO)$^+$BAr′$_4^-$

	3a	3b	3c	3d	3e	3f	3g
P−P	dppee	dpbz	dppe	dmpe	dppp	dippp	dppb
				^{1}H NMR			
[Pd]−C*H*$_3$[b]	0.90 (dd, 4, 4)	0.91 (dd, 4, 6)	0.73 (dd, 6, 4)	0.49 (dd, 5, 6)	0.48 (dd, 5, 5)	0.65 (dd, 6, 4)	0.70 (dd, 5, 5)
				^{13}C NMR			
[Pd]−*C*H$_3$[c]	1.8 (d, 70)	2.9 (d, 70)	1.5 (d, 70)	−4.8 (d, 74)	4.8 (d, 70)	−3.1 (d, 69)	5.8 (d, 70)
[Pd]−*C*O[c]	181.6 (dd, 119, 13)	181.7 (dd, 118, 12)	182.6 (dd, 148, 11)	182.3 (dd, 122, 13)	180.1 (dd, 118, 14)	182.6 (dd, 113, 14)	181.1 (br)
				^{31}P NMR			
(*P*−*P*)[Pd][d]	67.3 (d, 18)	57.1 (d, 30)	61.5 (d, 32)	41.4 (d, 30)	16.6 (d, 60)	23.7 (d, 67)	25.8 (d, 70)
	61.9 (d, 18)	48.0 (d, 30)	46.5 (d, 32)	30.1 (d, 30)	−7.9 (d, 60)	14.4 (d, 67)	1.6 (d, 70)
IR[e] (*ν*) [Pd]−CO	2136	2134	2133	*f*	2132	2122	2132

[a] Spectra were collected in CD_2Cl_2 at −80 °C. Chemical shift values (δ) are relative to CD_2Cl_2. All couplings (given in parentheses) are in Hz. [b] Couplings are $^3J_{HP}$. [c] Couplings are $^2J_{CP}$. [d] Couplings are $^2J_{PP}$. [e] CD_2Cl_2 solutions, given in cm^{-1}. [f] Decomposed.

Table 4. Selected NMR and IR Data[a] for (P−P)PdCOCH$_3$(CO)$^+$BAr′$_4^-$

	4a	4b	4c	4d	4e	4f	4g
P−P	dppee	dpbz	dppe	dmpe	dppp	dippp	dppb
				^{1}H NMR			
[Pd]−COC*H*$_3$[b]	1.6 (s)	2.06 (br)	1.97 (s)	2.54 (dd, 2, 1)	1.85 (s)	2.59 (s)	1.84 (s)
				^{13}C NMR			
[Pd]−CO*C*H$_3$[c]	42.0 (br)	42.0 (dd, 11, 30)	42.1 (dd, 38, 22)	45.1 (dd, 19, 38)	42.1 (dd, 24, 25)	45.9 (dd, 15, 36)	42.0 (dd, 21, 38)
[Pd]−*C*OCH$_3$[d]	222.0 (br)	232.5 (dd, 19, 87)	233.3 (br d, 150)	239.4 (dd, 5, 92)	232.0 (dd, 9, 85)	235.1 (dd, 6, 74)	229.4 (dd, 6, 84)
[Pd]−*C*O[d]	181.6 (dd, 12, 119)	179.0 (br)	177.2 (br d, 150)	181.0 (br)	175.7 (dd, 20, 83)	177.4 (dd, 20, 79)	175.3 (dd, 22, 80)
				^{31}P NMR			
(*P*−*P*)[Pd][e]	50.8 (d, 34)	39.2 (d, 50)	41.2 (d, 50)	26.8 (d, 47)	2.2 (d, 84)	23.7 (d, 67)	33.8 (d, 43)
	46.6 (d, 34)	38.5 (d, 50)	37.2 (d, 50)	19.7 (d, 47)	−8.0 (d, 84)	14.4 (d, 67)	18.7 (d, 43)
				IR[f] (*ν*)			
[Pd]−CO	2130	2132	2132	*g*	2130	2121	2130
[Pd]−acyl	1716	1716	1717	*g*	1715	1701	1719

[a] Spectra were collected in CD_2Cl_2 at −80 °C. Chemical shift values (δ) are relative to CD_2Cl_2. All couplings (given in parentheses) are in Hz. [b] Couplings are $^4J_{HP}$. [c] Couplings are $^3J_{CP}$. [d] Couplings are $^2J_{CP}$. [e] Couplings are $^2J_{PP}$. [f] CD_2Cl_2 solutions, given in cm^{-1}. [g] Decomposed.

phenanthroline)Pd(CH$_3$)(OEt$_2$)$^+$, in which both C−O bonds exhibit an anti conformation.[32] Examining the ORTEP diagrams reveals that this conformation likely results from the pseudoaxial phenyl groups forcing the methyl groups of the bound ether away from the metal center and into a gauche position.

3. Preparation of Methyl Carbonyl Complexes (P−P)Pd(CH$_3$)(CO)$^+$(BAr′$_4$)$^-$ (3a−g) and Kinetics of Their Migratory Insertion Reactions. Purging CH_2Cl_2 solutions of **2a−g** with CO at −90 °C results in immediate and quantitative conversion to **3a−g** (eq 5).

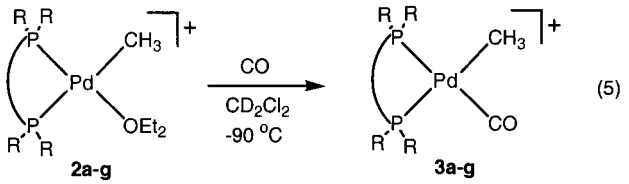

(5)

To avoid further reaction to acyl carbonyl complexes, excess CO was removed by purging each solution with argon at −90 °C. In the case of **3b−d** and **3e**, preparative-scale reactions could be carried out and the methyl carbonyl complexes isolated in good yields (77−95%) as thermally unstable solids (see the Supporting Information for synthetic details). ^{1}H, ^{13}C, and ^{31}P NMR spectroscopic analyses unambiguously established formation of the methyl carbonyl complexes (Table 3). All ^{1}H NMR resonances of the Pd−CH$_3$ groups appear between 0.5 and 1.0 ppm with ^{13}C signals in the −5 to 6 ppm range coupled to the trans ^{31}P by ca. 70 Hz. The ^{13}C{^{1}H} NMR resonances for the bound carbonyl ligand all appear around 180 ppm, with a large coupling to trans ^{31}P (113−148 Hz) and a small coupling to cis ^{31}P (11−14 Hz). In each case two ^{31}P{^{1}H} NMR signals appear as doublets with the low-field ^{31}P shift assigned to the phosphorus trans to CO.

When they are treated with various trapping ligands, L, the methyl carbonyl complexes undergo migratory insertion reactions to form acyl complexes of the type (P−P)Pd(L)(COCH$_3$)$^+$. For kinetic studies, CO has been employed as the trapping ligand, which results in the quantitative in situ formation of acyl carbonyl complexes (P−P)Pd(CO)(COCH$_3$)$^+$ (**4a−g**) (eq 6).

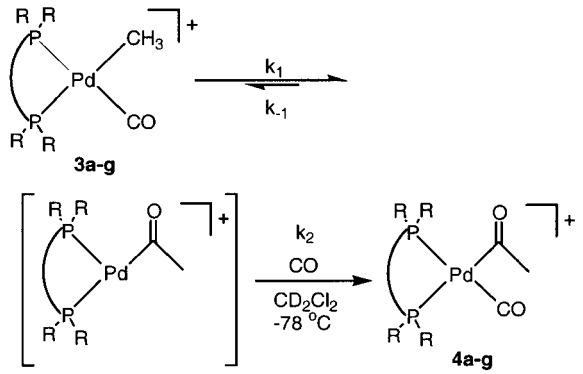

(6)

(32) Rix, F. C.; Brookhart, M.; White, P. S. *J. Am. Chem. Soc.* **1996**, *118*, 2436.

Table 5. Rate Data for the Migratory Insertion Reactions of the Methyl Carbonyl Complexes 3a−g

complex (ligand)	temp (K)	correlation coeff (r^2)	rate constant k_1 (10^4 s^{-1})	$\Delta G^{\ddagger}$ (kcal/mol)
3a (dppee)	238	0.996	18	17.1(2)
3b (dpbz)	232	0.998	4.23	17.1(2)
3c (dppe)	226	0.999	1.9	17.1(1)
3d (dmpe)	248	0.996	3.2	18.4(2)
3e (dppp)[a]	191	0.998	0.45	14.8(1)
3f (dippp)	191	0.994	3.4	14.1(2)
3g (dppb)	194	0.994	5.5	14.2(2)

[a] Data previously reported.[12]

Table 4 summarizes selected ^1H, ^{13}C, and ^{31}P NMR data for these acyl carbonyl complexes (CD_2Cl_2, −30 °C). The ^1H NMR shifts of the methyl groups move significantly downfield from the methyl carbonyl complexes and appear in the range of 1.8−2.6 ppm; ^{13}C NMR shifts also move downfield to 42−46 ppm. The $^{13}C\{^1H\}$ NMR resonances for the acyl carbon appear in the range of ca. 230−240 ppm, while the carbonyl ligands appear in the 175−180 ppm range, which is consistent with similar complexes (see the Supporting Information for complete spectroscopic details).[7,8,13,29,33] The acyl carbonyl complex (dppp)Pd(CO)(CH_3CO)$^+BAr'_4{}^-$ (**4e**) could be isolated in moderate yields (35%), as we have previously reported.[12] Attempts to isolate other carbonyl acyl complexes led to decarbonylated products.

Kinetics of conversion of the methyl carbonyl complexes to the acyl carbonyl complexes were conveniently followed by low-temperature $^1H\{^{31}P\}$ NMR spectroscopy in CD_2Cl_2 using the sharp, well-defined methyl resonances. Rates of conversion are independent of CO concentration and follow excellent first-order kinetics (see the Supporting Information for sample plots). Since CO solubility in CD_2Cl_2 is low, the concentrations of **3a**−**g** (ca. 4 μmol in 0.7 mL of CD_2Cl_2) must be kept low to ensure that conversions to the acyl carbonyl complexes are complete. First-order rate constants together with $\Delta G^{\ddagger}$ values for reactions are listed in Table 5. As with the (phen)Pd(CH_3)(CO)$^+$ system, the lack of dependence of the rate on CO concentration indicates that the migratory insertion step is rate-determining (k_2[CO] > k_{-1}, eq 6) and thus the rate constants in Table 5 represent the true rate constants (k_1) for migratory insertion of the methyl carbonyl complexes.[7,8]

An Eyring analysis for the migratory insertion reaction of (dppp)Pd(Me)(CO)$^+$ (**3e**) has been previously carried out and provides activation parameters for this process of $\Delta H^{\ddagger} = 14.8 \pm 0.7$ kcal/mol and $\Delta S^{\ddagger} = 0.1 \pm 3$ eu. The near-zero value of $\Delta S^{\ddagger}$ is consistent with the intramolecular nature of the migratory insertion, with no assistance from the solvent or additional equivalents of carbon monoxide.[34] That $\Delta S^{\ddagger}$ is ca. 0 implies that there is little temperature dependence of $\Delta G^{\ddagger}$ and thus over the limited temperature ranges given in Table 5 the $\Delta G^{\ddagger}$ values can be directly compared for the various methyl carbonyl complexes and, in addition, $\Delta H^{\ddagger}$ values will be close to $\Delta G^{\ddagger}$ values.

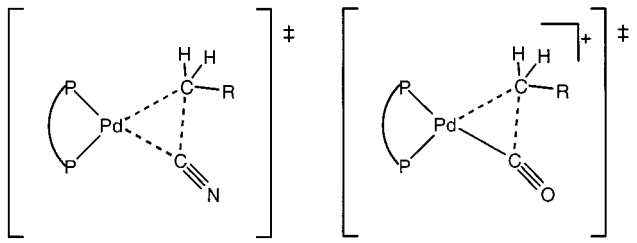

Figure 7. Possible transition state structures for reductive elimination of an alkyl cyanide complex and migratory insertion of an alkyl carbonyl complex.

The barriers measured for the methyl to carbonyl migratory insertion process clearly indicate that as the P−Pd−P bond angle of these complexes increases, the rate of reaction increases. For example, in the series [$Ph_2P(CH_2)_nPPh_2$]Pd(CH_3)(CO)$^+$ involving the dppe (n = 2), dppp (n = 3), and dppb (n = 4) ligands, the barrier decreases as n increases: 17.1 kcal/mol for n = 2, 14.8 kcal/mol for n = 3, and 14.2 kcal/mol for n = 4. The bond angles for [$Ph_2P(CH_2)_nPPh_2$]Pd(CH_3)(OEt_2)$^+$ are 102.4° for n = 4, 97.3° for n = 3, and a bond angle of ∼85° can be estimated for n = 2 on the basis of the literature structures.[31,35] The barriers for **3a**,**b**, containing two-carbon backbones, are quite similar (17.1 kcal/mol) to that of **3c**, which also has a two-carbon backbone. Complex **3d**, (dmpe)Pd(CH_3)(CO),$^+$ exhibits a barrier ca. 1.3 kcal/mol greater than **3a**−**c.** The Pd(II) center for this electron-rich phosphine is less electrophilic than that for **3a**−**c** and, in addition, the methyl substituents are less bulky than the aryl substituents; both factors would be expected to raise the barrier to migratory insertion. The dippp complex [(*i*-Pr_2)$P(CH_2)_3$P(*i*-Pr)$_2$]Pd(CH_3)(CO)$^+$ (**3f**) exhibits a somewhat lower barrier (14.1 kcal/mol) than **3e** (14.8 kcal/mol). On the basis of the electronic effects, the barrier of **3f** would be expected to be higher than for **3e**. The decrease in the barrier is best attributed to the bulkier nature of the isopropyl groups, which sterically crowd and destabilize the ground state more than do the aryl groups. This effect is dramatically illustrated in the next section, where such crowding by the isopropyl groups results in a change in the nature of the catalyst resting state for ethylene dimerization.

Moloy and co-workers have studied the reductive elimination reaction of a series of complexes of general formula (P−P)Pd(CH_2TMS)(CN) with various bidentate phosphine ligands.[36] These alkyl cyanide complexes are isoelectronic with the alkyl carbonyl complexes discussed here. In addition, the reductive elimination process should have a transition state very similar to that of the alkyl to carbonyl migratory insertion process (Figure 7). Moloy found that an increase in the ligand bond angle increased the rate of reductive elimination. Progressing from a small bond angle (∼85° for dppe) to a large bond angle (∼100° for DIOP) results in a nearly 10^4-fold increase in the rate of reductive elimination at 80 °C. In both types of processes an increase in ligand bond angle accompanies an increase in the steric influence of the ligand. Such increased steric demands compress the C−Pd−C angle, destabilizing the ground-

(33) Kayaki, Y.; Shimizu, I.; Yamamoto, A. *Bull. Chem. Soc. Jpn.* **1997**, *70*, 917.
(34) Collman, J. P.; Hegedus, L. S.; Norton, J. R.; Finke, R. G. *Principles and Applications of Organotransition Metal Chemistry*; University Science Books: Mill Valley, CA, 1987; Chapters 6, 11, 12.
(35) Steffen, W. L.; Palenik, G. J. *Inorg. Chem.* **1976**, *15*, 2432.
(36) Marcone, J. E.; Moloy, K. G. *J. Am. Chem. Soc.* **1998**, *120*, 8527.

Table 6. Selected NMR Data[a] for (P−P)PdCH$_3$(η^2-CH$_2$CH$_2$)$^+$BAr′$_4^-$

	5a	5b	5c	5d	5e	5f	5g
P−P	dppee	dpbz	dppe	dmpe	dppp	dippp	dppb
				^{1}H NMR			
[Pd]−C*H*$_3$[b]	0.85 (dd, 4, 6)	0.75 (dd, 3, 7)	0.61 (dd, 5, 5)	0.51 (dd, 5, 5)	0.32 (dd, 4,7)	0.35 (dd, 3, 6)	0.57 (dd, 7, 7)
[Pd](η^2-C*H*$_2$C*H*$_2$)	4.95 (br)	5.42 (br)	4.98 (br)	5.32 (br)	5.19 (br)	5.54 (br)	5.13 (br)
				^{31}P NMR			
(*P*−*P*)[Pd][d]	66.4 (d, 16)	51.4 (d, 30)	35.5 (br)	34.8 (d, 26)	17.6 (d, 56)	37.6 (d, 41)	35.3 (d, 55)
	75.8 (d, 16)	62.6 (d, 30)	13.5 (d, 32)	51.1 (d, 26)	−1.6 (d, 56)	7.3 (d, 41)	13.9 (d, 55)

[a] Spectra were collected in CD_2Cl_2 at −80 °C. Chemical shift values (δ) are relative to CD_2Cl_2. All couplings (given in parentheses) are in Hz. [b] Couplings are $^3J_{HP}$. [c] Couplings are $^2J_{CP}$. [d] Couplings are $^2J_{PP}$.

state structures. The expected result would be an acceleration in C−C bond formation.

4. Ethylene Dimerization Studies: Synthesis and Kinetics of the (P−P)Pd(η^2-C$_2$H$_4$)(R)$^+$BAr′$_4^-$ Complexes (R = Me, 5a−e,g; R = Et, 6a−e,g). The reaction of ether complexes **2a**−**e**,**g** with C_2H_4 in CD_2Cl_2 at −78 °C quantitatively generates the (P−P)PdMe(η^2-C_2H_4)$^+$BAr′$_4^-$ complexes **5a**−**e**,**g** (eq 7). The treatment of **2f** with ethylene is discussed later. These species are too unstable to be isolated but were completely characterized by NMR spectroscopy at low temperatures. Data are summarized in Table 6.

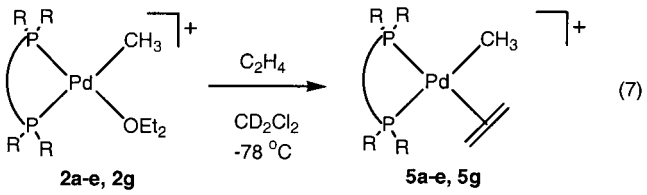

2a-e, 2g 5a-e, 5g (7)

For spectral characterizations, slightly less than 1 equiv of C_2H_4 was employed. If more than 1 equiv of C_2H_4 was added, exchange between complexed and free C_2H_4 results in broadened NMR signals. The ^{1}H NMR resonances of the Pd−CH_3 groups appear in the range of 0.3−0.8 ppm with a small coupling (4−7 Hz) to both ^{31}P nuclei. The ^{13}C resonances appear in the range of −2 to 19 ppm and exhibit a large trans J_{PC} (76−91 Hz) and small to unobservable cis J_{PC}. The ^{1}H NMR resonances of the η^2-ethylene ligands all appear as broad singlets (possibly due to exchange) between 5.0 and 5.5 ppm; the corresponding ^{13}C resonances are all in the range 99−110 ppm; in certain cases a small trans J_{PC} (5−10 Hz) can be observed.

When the methyl ethylene complexes are warmed to ca. −40 °C in the presence of excess ethylene, the clean conversion of **5a**−**e**,**g** to propylene and the ethyl ethylene complexes **6a**−**e**,**g** can be monitored (eq 8). With the exception of the dippp system (see below), the ethyl ethylene complex is the catalyst resting state for a catalytic cycle which dimerizes ethylene to butenes. This cycle is analogous to the one previously reported for the phenanthroline-based systems.[7,8] Quantitative rate measurements of the migratory insertion reactions of the methyl ethylene and ethyl ethylene complexes were made as described below.

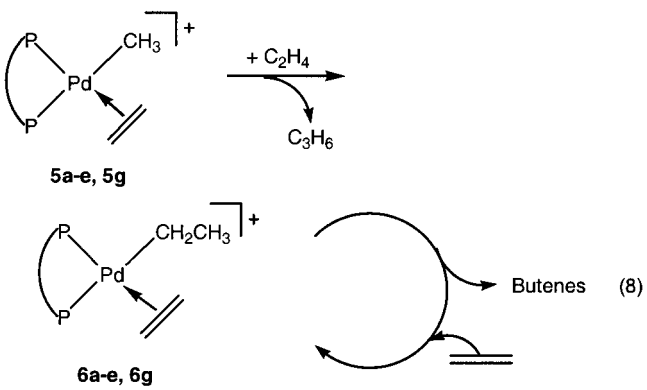

(8)

Table 7. Rate Data for the Migratory Insertion Reactions of the Methyl Ethylene Complexes 5a−g

complex (ligand)	temp (K)	correlation coeff (r^2)	rate constant k (10^4 s^{-1})[a]	$\Delta G^‡$ (kcal/mol)
5a (dppee)	237	0.991	4.2	17.4(2)
5b (dpbz)	232	0.997	8.1	16.8(2)
5c (dppe)	231	0.997	1.9	17.4(1)
5d (dmpe)	233	0.996	0.35	18.3(1)
5e (dppp)[b]	228	0.997	4.9	16.6(1)
5f (dippp)	229	0.997	10.2	16.5(2)
5g (dppb)	233	0.995	7.8	16.8(1)

[a] The rates were observed with 5−15 equiv of ethylene added; values are the average of at least two runs at each temperature. [b] Data previously reported.[12]

The rates of the migratory insertions of the methyl ethylene complexes **5a**−**e**,**g** were followed by monitoring the decrease in the Pd−CH_3 ^{1}H{^{31}P} NMR resonance. Clean first-order kinetics were observed, and rates were independent of the concentration of free ethylene in each case.[37] Kinetic data are summarized in Table 7.

As shown in eq 8, following migratory insertion of the methyl ethylene species, propylene is released and in the presence of excess ethylene, ethyl ethylene complexes are formed. NMR data are summarized in Table 8. These complexes are the only Pd species present in solution and are the catalyst resting states.[38]The turnover frequencies of the catalytic cycle are controlled by the rates of migratory insertion of these complexes, which can be easily obtained by measuring the rate of formation of butenes. These kinetic data are summarized in Table 9.

The $\Delta G^‡$ values for the methyl ethylene and ethyl ethylene migratory insertion processes are very similar, all being within 0.4 kcal/mol for the same ligand. Collectively the barriers for these alkyl ethylene complexes exhibit much less sensitivity to the P−Pd−P angle than do the methyl carbonyl complexes. For example, in the series [(C$_6$H$_5$)$_2$P(CH$_2$)$_n$P(C$_6$H$_5$)$_2$]Pd-

(37) For example, **5e(dppp)**: kinetic runs repeated at 227.6 K with 4, 9, and 19 equiv of ethylene give k_{obs} = 5.1 × 10^{-4}, 4.8 × 10^{-4}, and 4.9 × 10^{-4} s^{-1}. [Pd] = 9.7 mM in each case. [C_2H_4] = 39, 87, and 184 mM, respectively. [C_2H_4] was determined by integration.

(38) The dmpe complex **6d** exchanged with propylene at low ethylene concentrations and **6a**−**c**,**e**,**f** exchanged with 1-butene at low ethylene concentrations. The identity of (dmpe)PdEt(C_3H_7)$^+$ was confirmed by adding propylene to a sample of **6d**, (dmpe)PdEt(C_2H_4)$^+$ (^{31}P{^{1}H} NMR δ 41.0 (br), 23.0 (br)).

Table 8. Selected NMR Data[a] for (P−P)PdCH$_2$CH$_3$(η^2-CH$_2$CH$_2$)$^+$BAr′$_4^-$

	6a	6b	6c	6d	6e	6g
P−P	dppee	dpbz	dppe	dmpe	dppp	dppb
			^{1}H NMR			
[Pd]−CH$_2$C*H*$_3$	0.43 (br)	0.43 (br)	0.46 (br)	0.42 (br)	0.40 (br)	0.32 (br)
[Pd]−C*H*$_2$CH$_3$	2.06 (br)	1.98 (br)	1.74 (br)	1.43 (br)	1.42 (br)	1.91 (br)
[Pd](η^2-C*H*$_2$C*H*$_2$)	5.50 (br)	5.42 (br)	5.52 (br)	5.14 (br)	N/O	5.68 (br)
			^{31}P NMR			
(*P*−*P*)[Pd][b]	75.5 (d, 24)	59.0 (br)	48.8 (d, 38)	38.8 (br)	17.7 (d, 65)	24.2 (d, 52)
	62.9 (d, 24)	44.0 (br)	23.8 (d, 38)	23.0 (br)	−2.1 (d, 65)	22.8 (d, 52)

[a] Spectra were collected in CD_2Cl_2 at −80 °C. Chemical shift values (δ) are relative to CD_2Cl_2. All couplings (given in parentheses) are in Hz. [b] Couplings are $^2J_{PP}$.

Table 9. Rates and $\Delta G^{\ddagger}$ Values for the Migratory Insertion Reactions of Ethyl Ethylene Complexes 6a−c,e,g

complex (ligand)	temp (K)	correlation coeff (r^2)	TOF[a] (10^3 s^{-1})	$\Delta G^{\ddagger}$ (kcal/mol)
6a (dppee)	237	0.994	0.83	17.2(2)
6b (dpbz)	238	0.996	1.6	16.9(2)
6c (dppe)	244	0.994	1.6	17.3(1)
6d (dmpe)	250	0.999	1.3	17.9(2)
6e (dppp)[b]	237	0.997	5.5	16.3(1)
6g (dppb)	238	0.993	2.5	16.6(1)

[a] The turnover frequencies were observed with 5−15 equiv of ethylene added. [b] Data previously reported.[12]

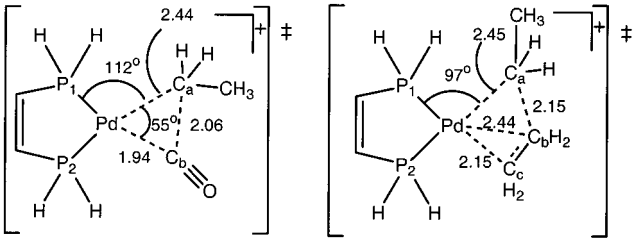

Figure 8. Transition state structures calculated by Ziegler et al.[19] for migratory insertions of (H$_2$PCH═CHPH$_2$)Pd(CH$_2$-CH$_3$)(CO)$^+$ and (H$_2$PCH═CHPH$_2$)Pd(CH$_2$CH$_3$)(CH$_2$CH$_2$)$^+$.

(CH$_3$)(C$_2$H$_4$)$^+$, the difference in $\Delta G^{\ddagger}$ values between **5g** (n = 4, 16.8 kcal/mol) and **5c** (n = 2, 17.4 kcal/mol) is only ca. 0.6 kcal/mol, whereas the difference is ca. 2.9 kcal/mol between the barriers in the analogous methyl carbonyl complexes. A similar trend is seen in the ethyl ethylene complexes **6g** and **6c**. The barrier to insertion in **5d**, (dmpe)Pd(CH$_3$)(C$_2$H$_4$)$^+$, is somewhat higher than that observed for the other complexes, no doubt due to a more electron rich diphosphine with reduced steric bulk.

The reduced response of the alkyl ethylene insertion barriers to change in the P−Pd−P bond angle can be rationalized on the basis of the contrasting ground- and transition-state structures for the methyl carbonyl and alkyl ethylene insertion reactions. Ziegler et al.[18,19] have calculated ground- and transition-state structures for model complexes in each system, employing H$_2$PCH═CHPH$_2$ as the bidentate phosphine. These transition-state models are illustrated in Figure 8. For the migratory insertion of the methyl carbonyl complex the C$_a$−Pd−C$_b$ angle is reduced 31° going from the ground state (86°) to the transition state (55°), while the P1−Pd−C$_a$ angle widens by 27° (85° to 112°). Thus, substantial sensitivity of the insertion barrier to the P−Pd−P bond angle would be expected through relief of steric crowding in the transition state. In the ground state of the ethyl ethylene complexes, the ethylene ligand lies perpendicular to the square plane; however, in the transition state for insertion, the ethylene ligand must rotate into the square plane and move three (not two as for aryl carbonyl complexes) carbon atoms within bonding distance of Pd. The square plane is now occupied by C$_a$, C$_b$, and C$_c$. This results in little reduction of steric crowding in the transition state relative to the ground state and may explain the reduced spread in barriers for insertions in the alkyl ethylene complexes. The calculated widening in the P$_1$−Pd−C$_a$ bond angle in the transition sate relative to the ground state is only 12° (85 to 97°) relative to the change of 27° in the methyl carbonyl complex.

5. Generation of (dippp)Pd(η^2-C$_2$H$_4$)(CH$_3$)$^+$BAr′$_4^-$ (5f) and (dippp)Pd(CH$_2$CH$_2$-μ-H)$^+$BAr′$_4^-$ (8f) and the Kinetics of Their Migratory Insertion Reactions. Analogous to the other systems employed in this study, the methyl ethylene complex **5f** containing the dippp ligand is cleanly generated by treating the ether adduct **2f** with ethylene at −78 °C. **5f** is too unstable to isolate but was completely characterized by NMR spectroscopy at low temperatures (Table 6).

When **5f** is warmed to ca. −44 °C in the presence of excess ethylene, the conversion to propylene and the β-ethyl agostic complex **8f** can be monitored (eq 9). Upon

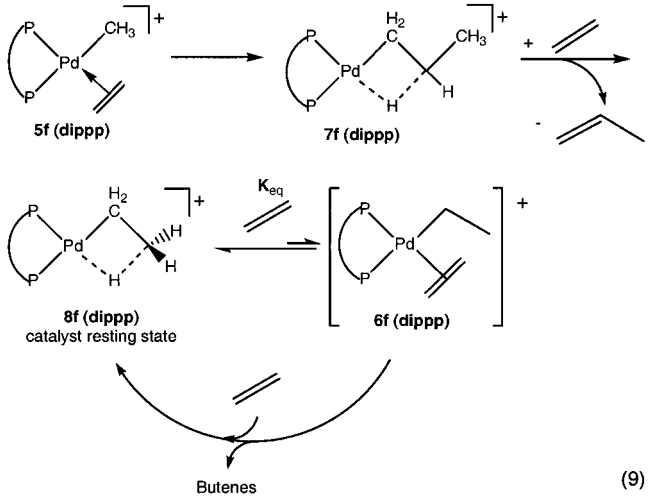

(9)

the initial migratory insertion of **5f** a transient species is generated which disappears as propylene is produced. We have assigned this transient complex as an agostic propyl complex, **7f**. If the solution is cooled to −120 °C, then a ^{1}H shift characteristic of an agostic hydrogen is observed at −2.71 ppm (br d, J_{PH} = 61 Hz). A detailed characterization of complex **7f** is described below. The rate of migratory insertion of complex **5f** was followed

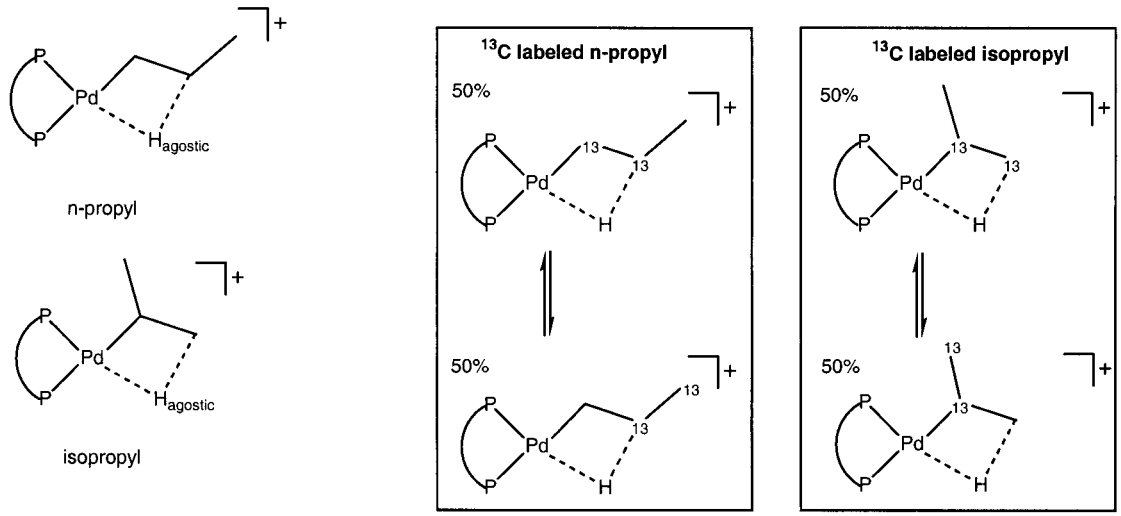

Figure 9. Characterization of *n*-propyl agostic complex **7f**.

by the decrease in the Pd−CH_3 $^1H\{^{31}P\}$ NMR resonance. This process was cleanly first order in **5f** and zero order in free ethylene. Kinetic data are summarized in Table 7.

The dippp system behaves very differently relative to the other systems examined with regard to ethylene dimerization. While the initial methyl ethylene complex, **5f**, undergoes migratory insertion to produce propylene at a rate comparable to that for **5e**,**g**, the second phase of the reaction, catalytic production of butenes, exhibits very different behavior, specifically (1) the dimerization reaction occurs at much slower rates than that for the other complexes examined, (2) the catalyst resting state is not an ethyl ethylene complex, and (3) the turnover frequency is now first-order in ethylene concentration. At 3 °C the second-order rate constant determined from the production of butenes is 1.58×10^{-3} M^{-1} s^{-1}. The catalyst resting state was successfully isolated from a catalytic reaction (see below) and shown to be the β-agostic species (dippp)Pd(CH_2CH_2-μ-H)$^+$ (**8f**). Thus, the catalytic cycle shown in eq 8 must be modified to account for these observations and is illustrated in eq 9. In this system, the bulky isopropyl substituents result in the less crowded agostic species **8f** being more stable under the reaction conditions than the much more crowded ethyl ethylene complex **6f**, in contrast to all other systems examined.

6. Characterization of the *n*-Propyl Agostic Complex (dippp)Pd(CH_2CH-μ-HCH_3)$^+$$BAr'_4{}^-$ (7f). Variable-temperature ^1H spectra of complex **7f** were complicated by the presence of free diethyl ether and the resonances of the dippp ligand in addition to broadening that arose from the low temperatures required to obtain static spectra (ca. −110 °C). Nevertheless, enough data could be extracted from NMR spectra of **7f** and **7f*** (generated using doubly ^{13}C labeled ethylene) to assign a structure to this complex. The ^1H spectrum of **7f** at −135 °C showed a resonance at −2.70 ppm (d, $^2J_{HP}$ = 61 Hz) that is consistent with an agostic hydrogen. **7f*** was next generated from doubly ^{13}C labeled ethylene. As shown in Figure 9, two possibilities arise with respect to the structure and labeling pattern of the propyl group of **7f***. If **7f*** is an agostic isopropyl species, then the carbon of the agostic methyl group will be 50% ^{13}C labeled due to rapid isomerization.[23,39] If **7f*** is an agostic *n*-propyl species, the carbon of the agostic methylene group (the central carbon) will be 100% ^{13}C labeled, since the isomerization process does not result in exchange of this carbon to a new site. The ^1H spectrum of **7f*** at −120 °C again showed the resonance at −2.70 ppm, now appearing to have triplet character. Decoupling ^{31}P from this spectrum caused this resonance to collapse to a doublet with $^1J_{CH}$ = 64 Hz, confirming the agostic nature of this hydrogen. No central peak is observed, indicating that $H_{agostic}$ is bound exclusively to a labeled carbon atom. This observation shows that the *n*-propyl agostic isomer of **7f** is the major isomer (>90%) in solution. This is in contrast to β-agostic (diimine)Pd−propyl$^+$ complexes where the agostic isopropyl species is favored over the *n*-propyl agostic species by ca. 20:1.[23,39] See the Supporting Information for full ^{13}C data of these complexes, which provide additional support for the proposed structures.

7. Isolation and Dynamic Solution Behavior of the Agostic Complex (dippp)Pd(CH_2CH_2-μ-H)$^+$-$BAr'_4{}^-$ (8f). Not only could the agostic complex **8f** be observed in situ during NMR-monitored catalytic dimerization reactions but it could also be isolated as a stable salt for spectroscopic studies. Purging a CH_2Cl_2 solution of **2f** with ethylene at 0 °C followed by solvent removal produced a yellow solid which, after recrystallization, gave **8f** as an analytically pure material. Cooling a $CDCl_2F$ solution of **8f** to −143 °C resulted in observation of a static $^1H\{^{31}P\}$ NMR spectrum with a resonance at −2.85 ppm assigned to an agostic hydrogen. Warming the solution results in rapid broadening of this signal due to rotation of the agostic methyl group (process **I**, Figure 10). A rate constant for methyl rotation can be estimated as 330 s^{-1} at −133 °C, corresponding to a $\Delta G^{\ddagger}$ value of ca. 6.4 kcal/mol. Warming to −68 °C results in coalescence (process **I**) of the two β-methylene hydrogens with the agostic hydrogen into a broad triplet (J = 7 Hz) at 0.05 ppm, integrated for three hydrogens. The α-methylene hydrogens appear at 1.75 ppm at these temperatures. Further warming to 5 °C results in coalescence of these two signals to a broad band at ca.

(39) Tempel, D. J.; Johnson, L. K.; Huff, R. L.; White, P. S.; Brookhart, M. *J. Am. Chem. Soc.* **2000**, *122*, 6686.

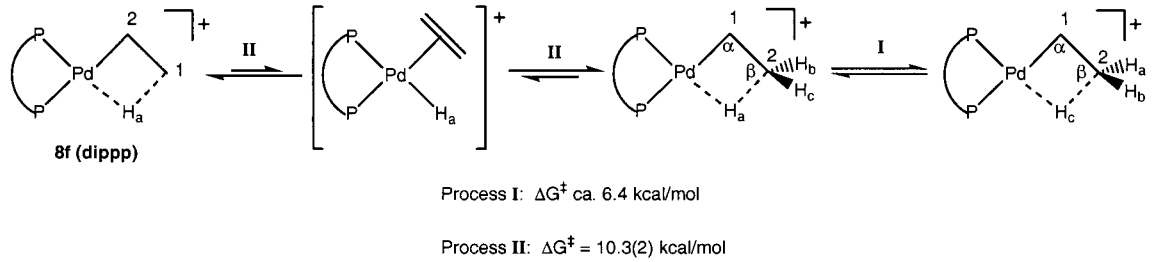

Figure 10. Fluxional processes observed for **8f** by $^{13}C\{^1H\}$ and ^1H NMR.

0.7 ppm, a result of the operation of both dynamic processes **I** and **II** shown in Figure 10. These processes together result in exchange of all five hydrogens of the agostic ethyl group. The barrier to β-H elimination and reinsertion (process **II**) could be estimated from broadening of the averaged agostic methyl group at both −58 and −44 °C as ca. 11(1) kcal/mol.

The activation barrier for β-H elimination and reinsertion (process **II**) could be more accurately determined using ^{13}C NMR spectroscopy, where the spectra are not affected by process **I**. The doubly ^{13}C-labeled agostic complex **8f***, prepared from $^{13}CH_2{=}^{13}CH_2$, exhibits two relatively sharp ^{13}C resonances at δ 27.7 and 6.9 ppm (−68 °C), assigned to C_a and C_b of **8f***, respectively. Decoupling experiments established that $^1J_{C_aH} = 157$ Hz, $J_{PC_a} = 34$ Hz, $J_{C_a-C_b} = 35$ Hz and $J_{CH(av)} = 123$ Hz for C_β. The averaged J_{CH} of the agostic methyl group of 123 Hz agrees with literature reports of analogous agostic complexes.[40−42] The coalescence temperature of the two ^{13}C resonances was observed to be −28 °C, and the rate constant for exchange was determined to be 3500 s^{-1} at −28 °C, with $\Delta G^‡ = 10.3(2)$ kcal/mol.

There is substantial precedent for species such as **8f** in the work of Spencer et al., who have observed similar Pt(II), Pd(II), and Ni(II) agostic ethyl complexes containing bidentate phosphine ligands.[40−43] Additionally, we have recently observed three other ethyl agostic complexes, two nickel(II) complexes of the general formula $[(P-P)Ni(CH_2CH_2\text{-}\mu\text{-}H)][X]$[44,45] and the palladium(II) complex $[(N-N)Pd(CH_2CH_2\text{-}\mu\text{-}H)][X]$.[46] The complex with the most similar dynamic NMR behavior to **8f**, however, is the $((t\text{-}Bu)_2P(CH_2)_3P(t\text{-}Bu)_2)Pt(CH_2\text{-}CH_2\text{-}\mu\text{-}H)^+$ complex.[40] The agostic proton resonance was observed as a broad signal at −2.6 ppm at −118 °C, and the ^{13}C NMR spectrum at −78 °C indicated C_α and C_β resonances at 28.3 and 6.1 ppm. As in **8f**, all five hydrogens of the agostic ethyl group appear as a broad singlet at 1.6 ppm at 25 °C due to rapid interchange via processes **I** and **II**.

Conclusions

A series of bidentate phosphine Pd(II) complexes that model the migratory insertion steps involved in the copolymerization of ethylene and CO have been examined. The kinetic barriers for the migratory insertion reactions of the series of complexes $[Ph_2P(CH_2)_nPPh_2]Pd(CH_3)(CO)^+$ ($n = 2-4$) decrease with increasing P−Pd−P bond angle of the complex for the ligands dppe ($n = 2$), dppp ($n = 3$), and dppb ($n = 4$). The rigidity of the ligand backbone appears to have little to no effect on this same process as is seen for the series of ligands dppe ≈ dpbz ≈ dppee. The steric bulk of the bisphosphine ligand had a significant effect on the methyl carbonyl insertion barriers, with the most bulky ligand (dippp) having the smallest activation barrier (14.1 kcal/mol) and the least bulky ligand (dmpe) having the largest activation barrier (18.4 kcal/mol).

In contrast to the methyl carbonyl case, the alkyl ethylene migratory insertion reactions experience very little if any significant increase in rate due to steric crowding or increase in the P−Pd−P bond angle. Following migratory insertion of $(P-P)Pd(CH_3)(C_2H_4)^+$ (**5a**−**e**,**g**) in the presence of ethylene, $(P-P)Pd(CH_2CH_3)(C_2H_4)^+$ (**6a**−**e**,**g**) are generated and are catalyst resting states for the zero-order dimerization of ethylene to butenes. The $(dippp)Pd(CH_3)(C_2H_4)^+$ complex, **5f**, has one of the lowest barriers to insertion, yet the subsequent rate of ethylene dimerization is greatly slowed due to a now first-order dependence on C_2H_4 concentration. The fact that the agostic ethyl complex **8f** is now the catalyst resting state explains the added dependence on ethylene. That the agostic ethyl complex is favored over the ethyl ethylene complex is likely due to the large steric bulk of the dippp ligand. These observations dramatically illustrate that subtle structural changes in a transition-metal complex can alter the catalyst resting state and greatly affect the rate and kinetic order of a catalytic reaction. The dynamic behavior of the agostic ethyl complex is notable in that the barriers to β-hydride elimination ($\Delta G^‡ = 10.3(2)$ kcal/mol, interchange of C_α, C_β) is substantially higher than the simple rotation of the agostic methyl group ($\Delta G^‡ =$ ca. 6.4 kcal/mol).

Experimental Section

General Methods. All reactions, except where indicated, were carried out in flame-dried glassware under a dry, oxygen-free argon atmosphere using standard Schlenk and drybox techniques. Acetone was degassed with argon and dried over 4 Å molecular sieves. All other solvents were either freshly distilled from sodium benzophenone or deoxygenated and then dried by passing them through a large column of activated alumina under nitrogen.[47] CD_2Cl_2 was purchased from Cambridge Isotope Laboratories, Inc. and dried over CaH_2 or P_4O_{10}.

(40) Conroy-Lewis, F. M.; Mole, L.; Redhouse, A. D.; Litster, A.; Spencer, J. L. *J. Chem. Soc., Chem. Commun.* **1991**, 1601.
(41) Spencer, J. L.; Mhinzi, G. S. *J. Chem. Soc., Dalton Trans.* **1995**, 3819.
(42) Mole, L.; Spencer, J. L.; Carr, N.; Orpen, A. G. *Organometallics* **1991**, *10*, 49.
(43) Carr, N.; Mole, L.; Orpen, A. G.; Spencer, J. L. *J. Chem. Soc., Dalton Trans.* **1992**, 2653.
(44) Shultz, C. S.; DeSimone, J. M.; Brookhart, M. *Organometallics* **2001**, *20*, 16.
(45) Shultz, C. S.; White, P. S.; DeSimone, J. M.; Brookhart, M. Manuscript in preparation.
(46) Shultz, L. H.; Brookhart, M. *Organometallics* **2001**, *20*, 3975.
(47) Pangborn, A. B.; Giardello, M. A.; Grubbs, R. H.; Rosen, R. K.; Timmers, F. J. *Organometallics* **1996**, *15*, 1518.

The CD_2Cl_2 was subjected to three freeze−pump−thaw cycles and vacuum-transferred into glass Schlenk tubes fitted with high-vacuum Teflon plugs and then stored under Ar. Air-sensitive complexes were handled in an Ar-filled drybox and stored under Ar at −30 °C. CP grade CO and ethylene were purchased from National Welders Supply and used as received. Ethylene-1,2-$^{13}C_2$, 99% ^{13}C, was purchased from Cambridge Isotope Laboratories, Inc., and used as received.

For complete details of the kinetics experiments see the Supporting Information. Kinetics experiments were carried out under Ar in NMR tubes equipped with septa. CD_2Cl_2 or $CDCl_2F$ was added to samples at −78 °C, after which solids were dissolved at the lowest temperature possible. Kinetics experiments were carried out on a Bruker AMX-300 or Avance 300 spectrometer. NMR probe temperatures were measured using an anhydrous methanol sample, except for temperatures below −95 °C, which were determined using a thermocouple.[48] ^1H and ^{13}C chemical shifts were referenced to residual ^1H signals and to the ^{13}C signals of the deuterated solvents, respectively.

Compounds **1b**, **1c**,[24,25,49] **1d**,[24,27] **1e**,[12,26] **1f**,[28] and **1g**[26] were synthesized in the same manner as **1a** (see the Supporting Information for details and spectroscopic analysis). Compound **2f**[2] was synthesized in the same manner as **2e** (see the Supporting Information for details and spectroscopic analysis). The syntheses and spectroscopic characterization of compounds **3e** and **4e** have been previously reported.[12] Elemental analyses were obtained from Oneida Research Services Inc., Whitesboro, NY, and Atlantic Microlabs Inc., Norcross, GA.

$H(OEt_2)_2BAr'_4$,[50] 1,3-bis(diisopropylphosphino)propane (dippp),[51] (TMEDA)$PdMe_2$ (TMEDA = *N*,*N*,*N*′,*N*′-tetramethylethylenediamine),[24] and $CDCl_2F$[52] were synthesized using published methods. The following phosphine ligands (>98% purity) were purchased from either Aldrich or Strem Chemicals and used as received: *cis*-1,2-bis(diphenylphosphino)ethylene (dppee), 1,2-bis(diphenylphosphino)benzene (dpbz), 1,2-bis(diphenylphosphino)ethane (dppe), 1,2-bis(dimethylphosphino)ethane (dmpe), 1,3-bis(diphenylphosphino)propane (dppp), and 1,4-bis(diphenylphosphino)butane (dppb).

The ^1H and ^{13}C NMR data attributed to the counterion $BAr'_4{}^-$ (Ar′ = 3,5-$(CF_3)_2C_6H_3$) are consistent for all cationic complexes examined and are not included in each compound characterized below. Full spectral details have been previously reported.[53]

Preparations. 1. Dimethyl Complexes 1a−f. The preparation of compound **1a** is given as a representative procedure for the synthesis of the series of dimethyl complexes **1a**−**f**. See the Supporting Information for specific details regarding the synthesis of compounds **1b**−**f**.

(dppee)$PdMe_2$ (1a). A method similar to van Koten's,[24] with only minor variations, was used to prepare all dimethyl complexes used in this study. A solution of dppee (0.266 g, 0.672 mmol) in acetone (15 mL) was added to a solution of (TMEDA)$PdMe_2$ (0.169 g, 0.671 mmol) in acetone (5 mL), and the mixture was stirred for 18 h. The solvent was removed in vacuo at 0 °C to yield a white precipitate. The precipitate was washed with hexanes (3 × 5 mL) and dried in vacuo to give complex **1a** (0.198 g, 55%). ^1H NMR (300 MHz, CD_2Cl_2, −60 °C): δ 7.32−7.51 (m, 22 H, $(C_6H_5)_2P(C_2H_2)P(C_6H_5)_2$), 0.25 (m, 6H, $Pd(CH_3)_2$). $^{13}C\{^1H,^{31}P\}$ NMR (75 MHz, CD_2Cl_2, −60 °C): δ 147.0 (P*C*H=*C*HP), 132.4, 132.3, 130.1, 128.6 ($(C_6H_5)_2P(C_2H_2)P(C_6H_5)_2$), −0.65 (Pd−*C*$H_3$). $^{31}P\{^1H\}$ NMR (121 MHz, CD_2Cl_2, −60 °C): δ 50.8. Anal. Calcd for $C_{28}H_{28}P_2Pd$: C, 63.11; H, 5.30. Found: C, 63.01; H, 5.35.

2. (P−P)PdMe$(OEt_2)^+(BAr'_4)^-$ (2a−f). The preparation of compound **2a** is given as a representative procedure for the synthesis of the series of **1a**−**f**. The preparation of the complex containing the dmpe ligand, **1d**, via this method was unsuccessful. See the Supporting Information for specific details regarding the synthesis of compounds **1b**,**c**,**e**,**f**.

(dppee)PdMe$(OEt_2)^+(BAr'_4)^-$ (2a). The dimethyl complex **1a** (0.125 g, 0.235 mmol) and $H(OEt_2)_2BAr'_4$ (0.255 g, 0.237 mmol) were suspended in ether (0.25 mL) and CH_2Cl_2 (0.75 mL) at −30 °C. The reaction mixture was stirred for 2 h, followed by brief warming to 25 °C in order to dissolve all solids. The resulting yellow solution was cooled slowly to −78 °C and stored overnight. The resulting precipitate was filtered and washed with pentane (2 × 3 mL) to afford complex **2a** (0.236 g, 69%) as a yellow powder. ^1H NMR (300 MHz, CD_2Cl_2, −60 °C): δ 7.46−7.62 (m, 20H, $(C_6H_5)_2PCHCHP(C_6H_5)_2$), 7.32 (br, 1H, P*CH*CHP), 7.15 (br, 1H, PCH*CH*P), 3.56 (br, 4H, $O(CH_2CH_3)_2$), 1.06 (br, 6H, $O(CH_2CH_3)_2$), 0.63 (d, $^3J_{HP}$ = 7.0, 3H, Pd−CH_3). $^{13}C\{^1H,^{31}P\}$ NMR (75 MHz, CD_2Cl_2, −60 °C): δ 146.4, 143.6 (P*C*H*C*HP), 132.6, 132.2, 132.1, 131.6, 129.8, 129.4, 128.1, 127.6 ($(C_6H_5)_2PCHCHP(C_6H_5)_2$), 70.2 ($O(CH_2CH_3)_2$), 15.5 ($O(CH_2CH_3)_2$), 12.3 (Pd−*C*$H_3$). $^{31}P\{^1H\}$ NMR (121 MHz, CD_2Cl_2, −60 °C): δ 61.2 (br), 49.2 (br). Anal. Calcd for $C_{63}H_{47}BF_{24}OP_2Pd$: C, 52.00; H, 3.26. Found: C, 52.14; H, 3.28.

(dippp)Pd$(CH_2CH_2$-μ-H)$^+(BAr'_4)^-$ (8f). Complex **2f** (0.270 g, 0.202 mmol) was dissolved in CH_2Cl_2 (1.5 mL) at 0 °C and purged with ethylene for 10 min. The solvent was removed in vacuo to afford a yellow solid. This yellow solid was redissolved in CH_2Cl_2 (1.0 mL) at 0 °C, and then the solution was slowly cooled to −78 °C and stored overnight. Colorless crystals of **8f** (0.18 g, 70%) were obtained. $^1H\{^{31}P\}$ NMR (300 MHz, $CDCl_2F$, −140 °C; at this temperature the ^1H resonances for the ligand, the α-methylene, and the two nonagostic hydrogens of the β-methyl group are all very broad and indistinguishable): δ −2.85 (br, 1H, Pd−CH_2CH_2−μ-*H*). $^1H\{^{31}P\}$ NMR (300 MHz, $CDCl_2F$, −68 °C): δ 2.07 (sept, 2H, $P(CH(CH_3)_2)_2$), 1.93 (sept, 2H, $P(CH(CH_3)_2)_2$), 1.75 (br q, 2H, $^3J_{HH}$ = 7, Pd−CH_2), 1.66 (br m, 2H, $PCH_2CH_2CH_2P$), 1.57 (br m, 2H, $PCH_2CH_2CH_2P$), 1.13 (br m, 2H, $PCH_2CH_2CH_2P$), 0.9 (br d, 24H, $((CH_3)_2CH)_2PCH_2CH_2CH_2P(CH(CH_3)_2)_2$, 0.05 (br t, 3H, $^3J_{HH}$ = 7, Pd−CH_2CH_3). $^1H\{^{31}P\}$ NMR (300 MHz, $CDCl_2F$, 5 °C): δ 2.07 (sept, 2H, $P(CH(CH_3)_2)_2$), 1.93 (sept, 2H, $P(CH(CH_3)_2)_2$), 1.66 (m, 2H, $PCH_2CH_2CH_2P$), 1.57 (m, 2H, $PCH_2CH_2CH_2P$), 1.13 (br m, 2H, $PCH_2CH_2CH_2P$), 0.9 (d, 24H, $((CH_3)_2CH)_2PCH_2CH_2CH_2P(CH(CH_3)_2)_2$), 0.7 (br, 5H, Pd−$CH_2CH_3$). $^{31}P\{^1H\}$ NMR (121 MHz, CD_2Cl_2, −68 °C): δ 50.5 (d, $^2J_{PP}$ = 42), 23.8 (d, $^2J_{PP}$ = 42). Anal. Calcd for $C_{49}H_{51}BF_{24}P_2Pd$: C, 46.16; H, 4.03. Found: C, 46.49; H, 3.97.

Acknowledgment. This work was supported by the U.S. Department of Energy and the National Science Foundation (Grant No. CHE-0107810).

Supporting Information Available: Text, figures, and tables giving full experimental details, sample kinetic plots, NMR data, and X-ray data. This material is available free of charge via the Internet at http://pubs.acs.org.

OM010489K

(48) Ammann, C.; Meier, P.; Merbach, A. E. *J. Magn. Reson.* **1982**, *46*, 319.
(49) Calvin, G.; Coates, G. E. *J. Chem. Soc.* **1960**, 2008.
(50) Brookhart, M.; Grant, B.; Volpe, A. F., Jr. *Organometallics* **1992**, *11*, 3920.
(51) Tani, K.; Tanigawa, E.; Tatsuno, Y.; Otsuka, S. *J. Organomet. Chem.* **1985**, *279*, 87.
(52) Siegel, J. S.; Anet, F. A. L. *J. Org. Chem.* **1988**, *53*, 2629.
(53) LaPointe, A.; Brookhart, M. *Organometallics* **1998**, *17*, 1530.